The Tasiast Deposit, Mauritania

Kyle HERON
Department of Geology, School of Natural Sciences, Trinity College, Dublin 2, Ireland
Mark JESSELL
Laboratoire GET, Université Toulouse 3 Paul Sabatier, IRD, CNRS UMR 5563, Observatoire Midi-Pyrénées, 31400 Toulouse, France and Centre for Exploration Targeting, The University of Western Australia, 35 Stirling Highway, Crawley, WA, 6009, Australia
Keith BENN
Terracognita Geological Consulting Inc., P. O. Box 100, 4874 St. Clair Parkway, Port Lambton, ON N0P 2B0, Canada
Esther HARRIS
Mineral Exploration Consultant, 96 Marlow St, Wembley, WA, 6014, Australia
Quentin G. CROWLEY
Department of Geology, School of Natural Sciences, Trinity College, Dublin 2, Ireland

ABSTRACT

The Tasiast gold deposits are hosted within Mesoarchean rocks of the Aouéouat greenstone belt, Mauritania. The Tasiast Mine consists of two deposits hosted within distinctly different rock types, both situated within the hanging wall of the west-vergent Tasiast thrust. The Piment deposits are hosted within metasedimentary rocks including metaturbidites and banded iron formation where the main mineral association consists of magnetite-quartz-pyrrhotite ± actinolite ± garnet ± biotite. Gold is associated with silica flooding and sulphide replacement of magnetite in the turbidites and in the banded iron formation units. The West Branch deposit is hosted within meta-igneous rocks, mainly diorites and quartz diorites that lie stratigraphically below host rocks of the Piment deposits. Most of the gold mineralisation at West Branch is hosted by quartz-carbonate veins within the sheared and hydrothermally altered meta-diorites that constitute the Greenschist Zone. At Tasiast, gold mineralisation has been defined over a strike length >10 km and to vertical depths of 740 m. All of the significant mineralised bodies defined to date dip moderately to steeply (45º to 70º) to the east and have a south-southeasterly plunge. Gold deposits on the Tasiast trend are associated with second order shear zones that are splays cutting the hanging wall block of the Tasiast thrust. An age of 2839 ± 36 Ma obtained from the hydrothermal overgrowth on zircons from a quartz vein is interpreted to represent the age of mineralisation.

Key words: Tasiast, Gold, Mauritania, BIF, Zircon geochronology

1. Introduction

There are 5 principal geological domains within the borders of Mauritania (Fig. 1a). The Reguibat Shield to the north of the country, hosts Archean and Palaeoproterozoic metamorphic sequences and granites that form the northwestern limit of the West African Craton (Ennih and Liegeois, 2008; Key et al., 2008). Further south the craton margin coincides with the Mauritanides, a Hercynian tectonic belt that consists of Neoproterozoic and Palaeozoic metamorphosed sediments and volcanoclastic formations and that also includes parts of the basement (Villeneuve, 2008). To the east of the Mauritanide belt lies the vast Mesoproterozoic (Teal and Kah, 2005; Rooney et al., 2010) to Palaeozoic Taoudeni basin. Finally to the West of the Mauritanides lies the northern limit of the Mauritania-Senegal-Gambia-Bissau-Conarky Basin, which is a Mesozoic-Cenozoic continental margin basin overlying a Palaeozoic (and probably Archean) basement.

Mauritania is a significant source of copper, gold, and iron ore and was the second ranked exporter and producer of iron ore in Africa, after South Africa, in 2012. In addition to iron ore, Mauritania produces cement, copper, crude oil, gold, gypsum, quartz, salt, and steel (Taib, 2012). The Tasiast gold deposit (location coordinates: 15.5124º W, 20.5786º N) is a >10 million ounce deposit located within the southwestern part of the Reguibat Shield, in the administrative region (Wilaya) of Inchiri, 250 km northeast of the capital Nouakchott.

Before discovery of the Tasiast deposit, the area had been subject to three regional exploration programs during the 1960s and 1970s with various non-gold targets as summarised in Table 1 (Stuart, 2010). The area was identified as being anomalous in gold during the first regional-scale geological mapping and geochemical sampling program of the European Development Fund project undertaken between 1993 and 1996 by the Bureau de Recherches Géologiques et Minières (BRGM) and the Office Mauritanien de Recherche Géologique (OMRG). The primary mission of the project was to locate new mineral indices of potential economic importance in the Tasiast area. More detailed soil sampling followed, resulting in the identification of a series of geochemical anomalies which were later tested by manual trenching. One of the soil geochemical anomalies, then called the C6-9 anomaly, eventually became the main Tasiast prospect (Stuart, 2010).

Exploration programs were conducted by a series of companies, beginning with Normandy La Source Development in 1996 who defined two principal areas of gold mineralisation within the Tasiast prospect (Mining Journal, 2006). Commercial production began in January 2008 when the mine was owned and operated by Red Back Mining B.V. (Stuart, 2010). The Tasiast mine is currently 100% owned and operated by the Kinross Gold Corporation. Kinross currently estimates the gold resource to be 12.8 million ounces at an average grade of 1.5 g/t (Table 2). In 2013, 2.5 Mt ore yielding 144,000 oz Au at a grade of 1.96 g/t in addition to 104,000 oz of dump leach gold for a total of 248,000 oz Au were produced (Table 3) (Sims, 2014).

2. Geological overview

The Tasiast gold deposit is located within one of three principal Precambrian greenstone belts that form part of the Tasiast-Tijirit Terrane located in the western part of the Reguibat Shield (Fig. 1a). The Reguibat Shield consists of a series of west to east accreted, north-south trending Archean and Paleoproterozoic metavolcano-sedimentary belts and domal basement gneiss complexes. The majority of rocks that have been dated in the Tasiast-Tijirit Terrane have been gneiss, TTG and granite samples, and are all between 2.97 Ga and 2.91 Ga in age (Chardon 1997, Key et al., 2008, Schofield et al., 2012; Gärtner et al., 2013, Montero et al., 2014). There have been two older TTG samples dated in the north of the region between 3.03 Ga and 3.01 Ga (Gärtner et al., 2013, Montero et al., 2014). The single other lithology to be dated in the region is a felsic volcanic obtained from drill core at the Tasiast deposit, which yielded an age of 2.97 Ga (Key et. al., 2008), which is currently the best constraint for the age of the host rocks at Tasiast. Although no crystallisation events older than 3.03 Ga are preserved in the Tasiast-Tijirit Terrane, whole rock Nd T_{DM} ages ranging from 3.60 Ga – 2.95 Ga (Chardon 1997, Key et al., 2008, Montero et al., 2014) suggest a contribution of older crustal material was involved in its creation.

The Aouéouat greenstone belt lies on the edge of one of a series of ENE oriented long-wavelength gravity and magnetic anomalies (Fig. 1b; Jessell et al., 2015). The Tasiast deposit is hosted within the north-south trending Aouéouat greenstone belt that is continuous for about 75 km strike length and shows as a series of high magnitude parallel anomalies in airborne magnetic data (Fig. 2b). The mine geology is characterized by a mafic to felsic meta-igneous succession, overlain by the remains of a sedimentary basin (Fig. 2a) that formed during rifting in a sinistral transtensional tectonic regime (Kruse, 2013). The preserved sedimentary stratigraphy includes abundant greywackes, siltstones, turbidite sequences and minor amounts of silica facies and possibly some oxide facies banded iron formations (BIF). The siliciclastic sedimentary rocks contain detritus derived from gneissic basement rocks as well as from younger volcanic and intrusive rocks that formed prior to the rifting event.

Gold mineralisation formed during the approximately E-W bulk shortening event that accompanied inversion of the Tasiast sedimentary basin (Fig. 3). That deformation resulted in tight to isoclinal, upright to overturned folds, thrusting and transcurrent shearing throughout the Aouéouat belt (Fig. 4a). According to the present understanding the Tasiast deposits were formed during that single, possibly transpressive tectonic event. In all the Piment deposits, gold is associated with silica flooding and sulfidation of magnetite. At West Branch, the gold is hosted by quartz-carbonate veins that are folded and locally transposed parallel to the principal foliation that is axial planar to the folds. Several families of northeast and northwest striking brittle faults crosscut the folds and locally offset geological units.

The rocks of the Aouéouat belt, including the host rocks of the Piment and West Branch deposits, preserve upper greenschist to lower amphibolite peak metamorphic mineral assemblages, and a younger supergene alteration history. Mineral parageneses including cordierite and andalusite indicative of HT-LP peak metamorphism have been locally identified within metasedimentary units and may be

associated with the emplacement of intrusive bodies of diorite and granodiorite compositions. Gold deposition occurred under middle greenschist post-peak metamorphic conditions as indicated by the presence of retrograde mineral assemblages including chlorite that are associated with mineralised veins and shear zones.

3. Gold mineralisation

The Tasiast Mine consists of two deposits hosted within distinctly different rock types. Both deposits are situated within the hanging wall block of the west vergent Tasiast thrust.

The Piment deposits are currently exploited as three main pits (North, Central and South) (Fig. 3) and are all hosted within metasedimentary rocks including metaturbidites and minor banded iron formation. Gold is associated with silicification and sulphide replacement of magnetite as observed within the turbidites and the banded iron formation units. In the Piment deposits the iron rich rocks represented a chemcially reactive host for gold mineralization. The alteration mineral assemblage is principally associated with brittle-ductile splay thrusts that branch off the Tasiast thrust.

i. The West Branch deposit hosts the bulk of the gold at Tasiast. It is hosted within meta-igneous rocks, predominantly diorites and quartz diorites that lie stratigraphically below the host rocks of the Piment deposits. The dioritic host rocks are situated within the core of an overturned antiformal fold and are bounded above and below by felsic metavolcanic rocks. The diorites are thought to have been the preferred host for gold because they represented a less ductile lithology that the enveloping felsic rocks, such that they efficiently localized high strains within shear zones that channeled fluids and that acted as structural traps. At West Branch several facies of veins are recognized within the so-called Greenschist Zone and include the following (in order of paragenesis):Early milky white quartz veins that are commonly tightly to isoclinally folded, and boudinaged at a low angle to the foliation.
ii. Quartz-albite-tourmaline veins that are also boudinaged at low angles to foliation.
iii. Greenish gray to translucent quartz ± native gold veins with a silica selvedge at low angles to foliation.
iv. Quartz-amphibole-biotite-carbonate-pyrite±garnet veins at low angles to the foliation.
v. Quartz-carbonate-biotite ± actinolite ± pyrite ± pyrrhotite ± tourmaline ± magnetite ± garnet veins that crosscut foliation at a high-angle.

The first four vein facies listed above are clearly syn-orogenic, probably having formed in extensional or shear fractures and were subsequently folded, boudinaged and locally transposed into the folation plane, or nearly so, during progressive deformation. Facies (i), (ii) and (iii) are observed to be cross-cut by veinlets of facies (iv) and visible gold is commonly associated with the carbonate-pyrite ± biotite rich veinlets. Facies (v) may be late orogenic, as those veins tend to be planar and undeformed to weakly deformed. The same facies of veins have been documented at satellite exploration targets along the Tasiast trend.

Metallic mineralogy within the Greenschist Zone is dominated by pyrrhotite, pyrite and native gold that occur as vein infill and alteration spots along the foliation, mainly in proximity to the veins. Pyrrhotite and pyrite occur together in many places but in variable ratios, with pyrrhotite being the predominant sulfide. Zones of pyrite-only and pyrrhotite-only mineralisation are rare. Blake (2011a, b in Sims, 2014) studied the nature, grain size and mode of occurrence of native gold grains in seven composites from two drill holes that intersected Greenschist Zone-style mineralisation. Results from the study concluded that the volume of coarse (>100 μm) Au grains account for the majority of contained Au and greater than 60% of grains occur in the liberated form and a lesser portion associated with gangue minerals and micrometre grains detected in slimes. At Piment the minerals of interest include native gold, pyrrhotite and pyrite.

Other sulphide minerals are recognized at both deposits in minor to trace abundances. These include electrum, chalcopyrite, arsenopyrite, sphalerite, galena, covellite, pentlandite and petzite.

4. Ore body characteristics

Gold mineralisation at the West Branch and Piment deposits has been defined over a strike length of about 10 km and to vertical depths of 740 m. Other mineralised exploration targets extend the strike length of the Tasiast camp several kilometres to the north and south. The deposits defined to date dip moderately to steeply (45º to 70º) to the east and have a south-southeasterly plunge; at some satellite exploration targets the mineralisation dips steeply to the west.

Piment mineralisation is largely hosted along splay faults and within the adjacent altered and veined iron formation and turbiditic units. Individual mineralised shoots are continuous over 300 m and to vertical depths of at least 260 m.

Most of the gold mineralisation at West Branch is hosted by quartz-carbonate veins in hydrothermally altered meta-diorites (Greenschist Zone, Fig. 4b). The meta-diorites are enveloped by a felsite unit that occurs on the footwall and hanging wall sides of the Greenschist zone, defining an overturned antiformal fold in the hanging wall of the Tasiast thrust. The Greenschist Zone is characterized by intervals of mineralisation averaging 40 m to 100 m in thickness. Individual shoots are continuous over a strike length of at least 1,000 m.

5. Geometric and kinematic controls

Gold mineralisation is associated with shear zones, quartz-veining (mainly at West Branch) and silica-flooding and sulphidation of magnetite (mainly at Piment, Fig. 4c). Gold deposits on the Tasiast trend are spatially associated with second order shear zones that are splay thrusts cutting the hanging wall block of the Tasiast thrust. Coarse visible gold is common within the quartz-carbonate veins (Fig. 4d).

Thrusting and tight to isoclinal folding has resulted in thickening of the stratigraphic package at Tasiast. The dominant foliation in the mine sequence is moderately to steeply east-dipping (45°-70°). Individual shear zones are typically 0.5 m to 10 m thick and are characterized by planar-laminated foliation with mylonitic textures locally observed. The shearing is commonly localised at contacts of lithologic units. The current structural interpretation of the mine area suggests that mineralisation is associated with second order shear zones that formed in the tightly to isoclinally folded rocks within the hanging wall of the west-vergent Tasiast thrust. The shear zones developed preferentially along the limbs of, and within the cores of very tight to isoclinal folds. Vein sets occur subparallel and oblique to foliation in styles that include boudinaged, buckled and planar.

6. Alteration

The following hydrothermal alteration and mineralisation history (Japan International Cooperation Agency (JICA)/OMRG, 2005) is thought to be a down-temperature time sequence, based on mineralogy and fluid inclusion analysis:

i. Tungsten mineralisation suggests a temperature maximum of about 280ºC. The salinity of the ore-forming fluid is assumed to have been about 37wt% NaCl eq and is thought to have been oxidising, based on chromium dissolution recognized in the tungsten mineralised region.
ii. White mica alteration occurred at a temperature of about 200ºC. Based on the clay mineralogy, the ore-forming fluid is assumed to have been neutral to weakly acidic, while intensive dissolution of iron from BIFs suggests it also acted as the reducing agent.
iii. Gold was produced at a temperature of about 150ºC. The salinity of the ore-forming fluid is assumed to have been about 26wt% NaCl eq.

Supergene alteration has resulted in an oxide zone characterized by leaching of quartz-carbonate veins and sulphides, and precipitation of calcrete and iron hydroxides in voids and fractures. No well-defined transition zone was identified as the strongly weathered upper portion of the deposits grades into fresh rock at depth. The depth of oxidation is in the order of 30 m to 60 m, at an average of 40 m. No supergene enrichment of gold is apparent in the upper profile.

7. Age of Mineralisation

Previous studies attempting to date the age of Tasiast mineralisation have relied on K-Ar dating of low potassium sericite, which gave an age of 1.9 Ga from a white argillized zone at the surface (Marutani et al., 2005). Dating of two distinct morphological types of hydrothermal monazite and xenotime from the Guelb Moghrein copper deposit yielded in situ U–Pb ages of 2492 ± 9 and 1742 ± 12 Ma respectively (Meyer et al., 2006) so a Meso-Proterozoic remobilisation remains a possibility in this part of the Reguibat Shield.

Apart from the results above, which do not seem to correlate with significant tectonic or magmatic activity in this region, there have been no previous attempts to directly date mineralisation at the Tasiast deposit. In order to address this we collected four samples of mineralised quartz veins from the Tasiast Mine and from several nearby exploration targets within the Aouéouat belt; three samples from drill core and one from an exploration trench. Three of these samples represent exploration target rocks, with the fourth being from the operational West Branch deposit. The primary purpose was to extract any minerals that could be used to date the formation of the quartz veins with a focus on hydrothermal zircon, monazite or xenotime. Zircon was separated from three of the four quartz veins, with the West Branch vein the only sample returning no zircons. Neither monazite nor xenotime were recovered from any of the samples.

Samples were crushed and zircons separated using standard techniques (Gemini water table, Frantz magnetic separation, and MI heavy-liquid separation), mounted in 1 inch diameter epoxy resin mounts, and polished to expose a near-equatorial section through the crystals. Analysis was carried out at the Geology Department, Trinity College Dublin, using Q-LA-ICP-MS (Thermo Scientific iCAP Qs, Photon Machines 193 nm ArF Excimer laser; see Crowley et al. (2014) for operating conditions). Zircon 91500 (Wiedenbeck et al., 1995) was used as the primary standard, with Plešovice (Sláma et al., 2008) and Temora (Black et al., 2003) as secondary standards. The VizualAge data reduction scheme (Petrus and Kamber, 2012) within Iolite (Paton et al., 2011) was used to process data and Isoplot 4.15 (Ludwig, 2003) was used for data plotting. It is worth noting a large proportion of zircons analysed are discordant in nature, exhibiting varying degrees of Pb-loss. This is not unusual in Archean and Proterozoic terranes, and has been apparent in previous studies on the Tasiast-Tijirit Terrane (e.g. Key et al., 2008, Gärtner et al., 2013). The results of U-Pb dating from the three quartz veins containing zircon are presented below, and in Supplementary Material Table 1.

TSUPB015, Quartz-Carbonate Vein (Drill Collar Location 446500, 2282415 UTM WGS84 Zone 28Q)

TSUPB015 is a sample of drill core from a hole located 5 km north of the Piment deposits in target C6.7 and it yielded 43 zircons (Fig. 5a). The vein includes facies (iii) cross-cut by facies (iv). CL-images of the zircons show oscillatory zoning in most indicating they are igneous in nature, with metamict cores present in some (Fig. 6a). The zircons are therefore almost certainly xenocrystic. A number of zircons possess an extremely thin (<10 μm) overgrowth seen by the dark CL rim surrounding the zircon on all sides (Fig. 6a), interpreted as hydrothermal in origin. Of the 43 zircon analyses, 15 were <10 % discordant, with Concordia ages of 3037 ± 29 Ma and 2946 ± 26 Ma obtained from time-resolved components of these least discordant analyses. A further two analyses overlapping with Concordia were obtained from this sample, with Concordia ages of 2819 ± 19 and 2695 ± 18 Ma, the latter of which is attributed to Pb-loss (Fig. 7a).

TSUPB016, Quartz-Carbonate Vein (Drill Collar Location 450250 2273595 UTM WGS84 Zone 28Q)

TSUPB016 is a sample of drill core from a hole located 5 km east of the Piment deposits in target C6.12 and yielded 48 zircons (Fig. 5b). The vein is of the tourmaline bearing facies (ii). CL-images

show oscillatory zoning again with some metamict cores indicating these too are xenocrystic, however none show evidence of hydrothermal overgrowths (Fig. 6b). This is confirmed by the U-Pb data, with the 14 analyses <10 % discordant containing one concordant population at 2953 ± 11 Ma (Fig. 7b), and a total range of $^{207}Pb/^{206}Pb$ ages of c. 3080 – 2945 Ma (Fig. 7c).

TSUPB026, Quartz-Carbonate Vein (Outcrop Location 445849 2284695 UTM WGS84 Zone 28Q)

TSUPB026 was collected as a field sample of a quartz vein from an exploration trench in the Fennec target, 10 km north of the Piment deposits (Fig. 4e, 5c). The sample exhibited strong signs of weathering, breaking apart where transected by thin carbonate veinlets. The quartz itself however remained intact. The vein includes facies (iii) cross-cut by facies (iv). This sample, partially due to the ability to obtain a larger volume of rock than from drill core, yielded ample zircon, and so an initial set of 104 grains were analysed. CL-images show igneous zircon with oscillatory zoning, some with more complex zoning, and a number possessing cores (Fig. 6c). All zircons from this sample had an obvious, generally <10 µ thick, overgrowth which again has been interpreted as hydrothermal in origin. The entire population gave an upper-intercept age of 2950 ± 11 Ma, with six zircons <10% discordant giving an upper intercept age of 2958 Ma ± 14 Ma (MSWD = 0.92) which is the preferred age for this sample (Figs. 7d & 7e).

Due to the ubiquitous presence of hydrothermal overgrowths on the zircons extracted from this sample, a second set of ten zircons were hand-picked, pre-treated in dilute HNO_3, and mounted on double-sided sticky tape without polishing. The exterior crystal faces were then ablated in two-second increments in an attempt to sample only the hydrothermal overgrowths. Five of the ten analyses exhibited extreme Pb-loss resulting in errors >140 Ma, which was not unexpected, since the rim of a zircon is the most likely part of a crystal to be affected by Pb-loss (Krogh, 1982). Three analyses did not produce any meaningful data and one sample gave a similar age to those obtained above, highlighting the lack of an overgrowth. This left one analysis providing usable data. An upper-intercept age of the two-second increments gave an age of 2839 ± 36 Ma (Fig. 7f).

The ages between c. 3060 and 2945 Ma obtained from all three quartz veins are interpreted as xenocrystic inherited zircons from neighbouring country rocks, or from deeper unexposed rock, and so provide a window on the ages of rocks present in the Aouéouat stratigraphy. Most of these ages overlap within error of previous ages obtained from the Tasiast-Tijirit Terrane gneiss and TTG rocks (Chardon 1997, Key et al., 2008, Gärtner et al., 2013, Montero et al., 2014) which confirms this interpretation. The minor older component, up to 3080 Ma is within error of zircon T_{DM} Hf model ages (c. 3080 to 3030 Ma) calculated from c. 2950 to 2910 Ma granitic and TTG intrusions in the Tasiast-Tijirit Terrane (Key et al., 2008). The 2839 ± 36 Ma age obtained from the hydrothermal overgrowth from the Fennec sample is within error of a concordant age obtained from C6.7 (2819 ± 19 Ma). The dated vein is of a known visible gold bearing generation. This age is interpreted as the crystallisation age of the hydrothermal quartz veins, and therefore the mineralisation age of the Tasiast deposit.

8. Summary

The Tasiast gold deposit is situated on the flank of a long-wavelength gravity ENE oriented gravity high and a north-south oriented BIF which appears clearly in regional aeromagnetic data. The deposit mineralisation is focused in splay shears off the west-vergent Tasiast thrust and is associated with an alteration sequence interpreted to show a down-temperature evolution with time. Mineralization is controlled by both chemical traps (especially at the Piment deposits) and structural traps (shear zones),, epigenetic in style and was coincident with early stages of post-peak metamorphic retrograde greenschist P-T conditions. An age of 2839 ± 36 Ma obtained from the hydrothermal overgrowth on zircons from a quartz vein is interpreted to represent the age of mineralisation.

Acknowledgements

Our thanks go to Kim Hein for improvements to the manuscript. We wish to gratefully acknowledge AMIRA International and the industry sponsors, as well as AusAID and the ARC Linkage Project LP110100667, for their support of the WAXI project (P934A). We are also appreciative of the contribution of the various Geological Surveys/Department of Mines in West Africa as sponsors in kind of WAXI. We wish to recognize our WAXI research colleagues from the various Institutions from around the world. We would like to thank SIGM for their permission to republish PRISM geological maps and magnetic data. We acknowledge the use of gravity data supplied by the BGI. Finally our thanks go to Kinross Gold Corporation for their permission to publish this paper.

References

Black, L.P., Kamo, S.L., Allen, C.M., Aleinikoff, J.N., Davis, D.W., Korsch, R.J., Foudoulis, C. 2003. TEMORA 1: a new zircon standard for Phanerozoic U–Pb geochronology. Chemical Geology 200, 155–170.

Blake, C. 2011a. Mineralogical characterisation of five gold-bearing samples from the Tasiast mine, Mauritania for Kinross Gold Corporation. Internal unpublished report (February, 2011).

Blake, C. 2011b. Mineralogical characterisation of seven gold-bearing composite samples from the Tasiast Mine, Mauritania for Kinross Gold Corporation. Internal unpublished report (September, 2011).

Chardon, D. 1997. Les deformations continentals Archéennes. Examples naturels et modèlisation thermomécanique. Mémoires de Géosciences, Rennes, 76.

Chorlton, L.B. 2007. Generalized geology of the world: bedrock domains and major faults in GIS 416 format: a small-scale world geology map with an extended geological attribute database. 417 Geological Survey of Canada, Open File 5529, 2007; 48 pages; 1 CD-ROM, 418 doi:10.4095/223767.

Crowley, Q.G., Heron, K., Riggs, N., Kamber, B. Chew, D., McConnell, B., Benn, K. 2014. Chemical Abrasion Applied to LA-ICP-MS U–Pb Zircon Geochronology. Minerals 4, 503-518.

Ennih, N., Liegeois, J.-P. (eds) 2008. The Boundaries of the West African Craton. Geological Society, London, Special Publications, 297.

Gärtner, A., Villeneuve, M., Linnemann, U., Archi, A.E., Hervé, B. 2013. An exotic terrane of Laurussian affinity in the Mauritanides and Souttoufides (Moroccan Sahara). Gondwana Research 24, 687–699.

Jessell, M.W., Begg, G.C., Miller, M.S. 2015. The Geophysical Signatures of the West African Craton. in press, Precambrian Research, doi: 10.1016/j.precamres.2015.08.010.

JICA/OMRG Report on the Tasiast Gold Deposit. 2005. http://www.omrg.mr/spip.php?article88

Key, R.M., Loughlin, S.C., Horstwood, M.S.A., Gillespie, M., Pitfield, P.E.J., Henney, P.J., Crowley, Q.G., Del Rio, M. 2008. Two Mesoarchaean terranes in the Reguibat shield of NW Mauritania. In: Ennih, N., Liégeois, J.-P. (Eds.), Boundaries of the West African Craton, vol. 297. Special Publication of the Geological Society, London, pp. 33–52.

Krogh, T.E. 1982. Improved accuracy of U-Pb zircon ages by the creation of more concordant systems using an air abrasion technique. Geochimica et Cosmochimica Acta. Vol 46, pp 637-649.

Kruse, S., 2013. Regional geometry and tectonic evolution of the Aouéouat greenstone belt and Tasiast metallogenic district. Unpublished Internal Report for Kinross Tasiast, Terrane Geoscience Inc.

Ludwig, K.R. 2003. Isoplot 3.00: A geochronological toolkit for Microsoft Excel. Berkeley. Geochronology Centre Special Publication 4, 0–71.

354 Marutani, M., Higashihara, M., Watanabe, Y., Murakami, H., Kojima G., Dioumassi, B. 2005. Metallic
355 ore deposits in the Islamic Republic of Mauritania. Resource Geology, 55, 59-70.
356 Meyer, F.M., Kolb, J., Sakellaris, G.A., Gerdes, A. 2006. New ages from the Mauritanides Belt:
357 recognition of Archean IOCG mineralization at Guelb Moghrein, Mauritania, Terra Nova, 18,
358 345–352.
359 Mining Journal. 2006. Mauritania: London, Mining Journal Special Publication, February 2006, 12 p.
360 Montero, P., Haissen, F., Archi, A.E., Rjimati, E., Bea, F. 2014. Timing of Archean crust formation and
361 cratonisation in the Awsard-Tichla zone of the NW Reguibat Rise, West African Craton. A
362 SHRIMP, Nd-Sr isotopes, and geochemical reconnaissance study, Precambrian Research, 242,
363 112-137.
364 Paton, C., Hellstrom, J., Paul, B., Woodhead, J., Hergt, J. 2011. Iolite: Freeware for the visualisation
365 and processing of mass spectrometric data. Journal of Analytical Atomic Spectrometry. 26, 2508-
366 2518.
367 Petrus, J.A., Kamber, B.S. 2012. Vizualage: A novel approach to laser ablation ICP-MS U-Pb
368 geochronology data reduction. Geostandards and Geoanalytical Research. 36, 247-270.
369 Rooney, A.D., Selby, D., Houzay, J.-P., Renne, P.R. 2010. Re–Os geochronology of a Mesoproterozoic
370 sedimentary succession, Taoudeni basin, Mauritania: Implications for basin wide correlations
371 and Re–Os organic-rich sediments systematic. Earth and Planetary Science Letters, v. 289, no.
372 3-4, pp. 486-496.
373 Schofield, D.I., Horstwood, M.S.A., Pitfield, P.E.J., Gillespie, M., Darbyshire, F., O'Connor, E.A.,
374 Abdouloye, T.B. 2012. U–Pb dating and Sm–Nd isotopic analysis of granitic rocks from the Tiris
375 Complex: New constaints on key events in the evolution of the Reguibat Shield, Mauritania.
376 Precambrian Research, 204-205, 1–11. doi:10.1016/j.precamres.2011.12.008.
377 Sims, J. 2014. Tasiast Project Mauritania National Instrument 43-101 Technical Report, prepared for
378 Kinross Gold Corporation. 253p.
379 Sláma, J., Košler, J., Condon, D.J., Crowley, J.L., Gerdes, A., Hanchar, J.M., Horstwood, M.S., Morris,
380 G.A., Nasdala, L., Norberg, N. 2008. Plešovice zircon—a new natural reference material for U–
381 Pb and Hf isotopic microanalysis. Chemical Geology. 249, 1-35.
382 Stuart, H. 2010. Technical Report on the Tasiast Gold Mine Islamic Republic of Mauritania for Red
383 Back Mining Inc.: unpublished technical report prepared for Red Back Mining Inc., effective
384 date 6 September 2010. 104p.
385 Taib, M. 2012. The Mineral Industry of Mauritania, USGS Minerals Yearbook 2012 (Advance
386 Release). 6p.
387 Teal, D.J., Kah, L.C., 2005. Using C-isotopes to constrain interbasinal stratigraphic correlations,
388 Mesoproterozoic Atar Group, Mauritania. Geological Society of America, Abstracts with
389 Programs 37, 45.

Villeneuve, M. 2008. Review of the orogenic belts on the western side of the West African craton: the Bassarides, Rokelides and Mauritanides. In: Ennih, N., Liégeois, J.-P. (Eds.), Boundaries of the West African Craton, vol. 297. Special Publication of the Geological Society, London, pp. 169–201.

Wiedenbeck, M., Alle, P., Corfu, F., Griffin, W., Meier, M., Oberli, F., Quadt, A.v., Roddick, J., Spiegel, W. 1995. Three natural zircon standards for U-Th-Pb, Lu-Hf, trace element and REE analyses. Geostandards newsletter. 19, 1-23.

400 **Table 1: Early exploration history of the Tasiast region (after Stuart, 2010)**

Period	Operator	Activity	Exploration Scale
1962-1963	BRGM	The pegmatite Mission (for Be and Li)	Regional
1972	BRGM	Nickel Sulphide Mission	Regional
1973-1975	SNIM	Iron Ore Mission	Regional
1993-1996	BRGM + OMRG	European Development Fund project	Regional and infill

BRGM - Bureau de Recherches Géologique et Minières (French Geological Survey)
SNIM - Société Nationale Industrielle et Minière (Majority Mauritanian State-owned mining company)
OMRG - Office Mauritanien de Recherches Géologiques (Mauritanian Geological Survey)

Table 2 Mineral Reserve and Resource Summary
As at December 31, 2014

Gold	**Tonnes (X 1,000)**	**Grade (g/t)**	**Ounces (X 1,000)**
Proven and Probable Reserves	161,822	1.77	9,196
Measured and Indicated Resources (*a*)	85,573	1.14	3,148
Inferred Resources	8,915	1.71	492
Total (*b*)	**256,310**	**1.56**	**12,836**

a) Measured and Indicated Resources exclude Proven and Probable Reserves
b) 'Total' Grade is the weighted average of the three cited grades according to Tonnes
After www.kinross.com/ operations/operation-tasiast-mauritania.aspx

Table 3 Production Summary

Year	**Tonnes Milled (Mt)**	**Grade (g/t)**	**Gold Produced ('000 oz.)**	Dump Leach Gold **Produced ('000 oz.)**	Total **Gold Produced ('000 oz.)**
2013	2.50	1.96	144	104	248
2012	2.55	1.54	114	71	185
2011	2.61	2.53	153	48	201
2010	2.14	2.46	151	36	187
2009	1.69	2.87	143	16	159
2008	1.49	3.10	140	0	140
2007	0.22	4.77	21	0	21

401 Table 3 from Sims, 2014.

402

403

Figure 1. a) Geological Framework of the West African Craton, showing the location of the Tasiast deposit (gold) in Mauritania, together with the ages of the major terranes, modified from the Geological Survey of Canada 1:35M map of the world (Chorlton, 2007). The approximate limit of the present day WAC is shown as a heavy dashed line (after Ennih and Liegeois, 2008), and the limit of the gravity data shown in Figure 1b is shown as a dotted rectangle. Two-letter country codes: BF: Burkina Faso; CI: Côte d'Ivoire; DZ: Algeria; GH: Ghana; GM: The Gambia; GN: Guinea; GW: Guinea Bissau; LR: Liberia; MA: Morocco; ML: Mali; MR: Mauritania; NE: Niger; SL: Sierra Leone; SN: Senegal; and TO: Togo. b) Free Air gravity image of Northern Mauritania showing location of principal deposits.

Figure 2. a) Geological setting of the Tasiast deposit, (After PRISM 1:500k geological map). b) First Vertical Derivative of the Reduced to the Pole airborne magnetic data. The principal anomalies seen are the NNW traces of the BIFs, together with two sets of dykes, one solitary dyke trending NW just north of the Tasiast deposit, and a dense swarm of dykes trending N to NE that obscure much of the geological signal.

Figure 3. Location of principal deposits and their host rocks, as well as the main structural features (After Stuart 2010).

Figure 4. a) Isoclinally folded sediments that are representative of the host rocks for all the Piment deposits, Tasiast Mine, pen for scale.. b) Strongly foliated meta-diorite from West Branch typical of the Greenschist Zone. c) Silica flooding and extensive sulphide mineralisation, mainly pyrrhotite, parallel to bedding in the metaturbidites at Piment. d) Visible gold hosted in a quartz-carbonate vein, in drill core taken from the West Branch deposit. e) Field location of quartz-carbonate vein TSUPB026. All core is 63.5 mm in diameter.

Figure 5. Samples used for zircon analysis. a) TSUPB015 is a sample of drill core from a hole located 7 km north of the Piment Central deposit in target C6.7 showing pervasive quartz-carbonate veining. b) TSUPB016 is a sample of drill core from a hole located 4 km east of the Piment deposits in target C6.12, showing pervasive quartz-carbonate veining. c) TSUPB026 was collected as a field sample of a quartz-carbonate vein from an exploration trench in the Fennec target, 10 km north of the Piment deposits. All core is 63.5 mm in diameter.

Figure 6. Representative CL-images of zircons used for U-Pb dating. a) TSUPB015 CL-images show oscillatory zoning in most grains indicating they are igneous in nature, with some showing metamict cores. Some of these xenocrystic zircons show a thin (<10 μm) overgrowth seen by the dark CL rim surrounding the zircon on all sides, interpreted as hydrothermal in origin. b) TSUPB016 CL-images show oscillatory zoning with some metamict cores indicating they are xenocrystic, however none show

evidence of hydrothermal overgrowths. c) TSUPB026 sample CL-images show igneous zircon with oscillatory zoning, some with more complex zoning, and a number possessing cores. All zircons from this sample had an obvious, generally <10 µ thick, overgrowth which is interpreted as hydrothermal in origin.

Figure 7. U-Pb Concordia plots a) TSUPB015 analyses <10 % discordant. b) TSUPB016 upper-intercept plot of concordant population. c) TSUPB016 analyses <10 % discordant. d) TSUPB026. e) TSUPB026 upper intercept plot of analyses <10 % discordant. f) TSUPB026 upper-intercept plot of hydrothermal overgrowth.

Table 1: Early exploration history of the Tasiast region (after Stuart, 2010).

Table 2 Mineral Reserve and Resource Summary (From Kinross Annual Report 2014).

Table 3 Production Summary (From Sims, 2014)

Supplementary Material

SM Table 1 U-Pb zircon data.

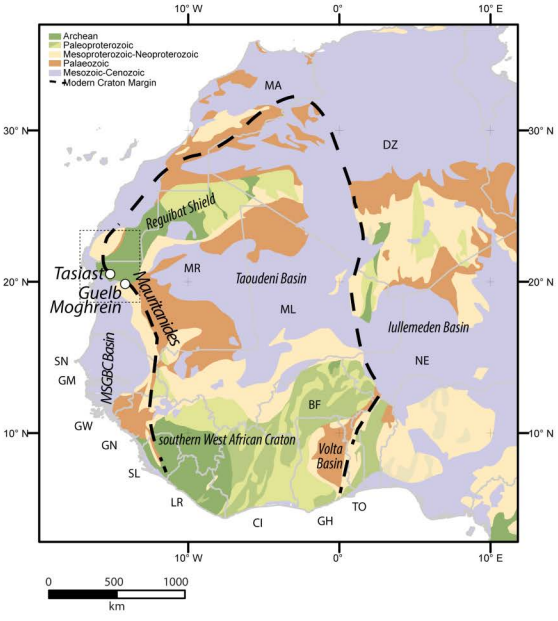

Figure 1a

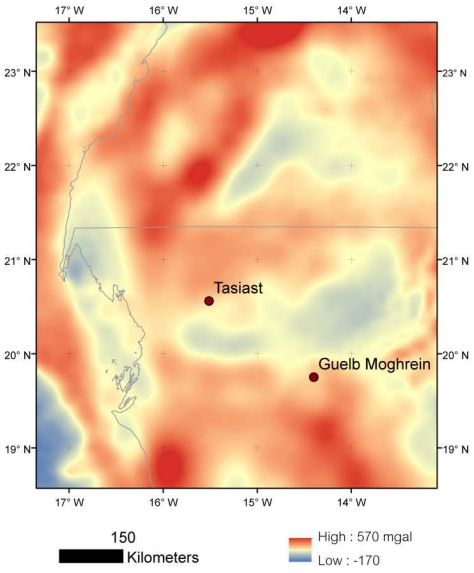

Figure 1b

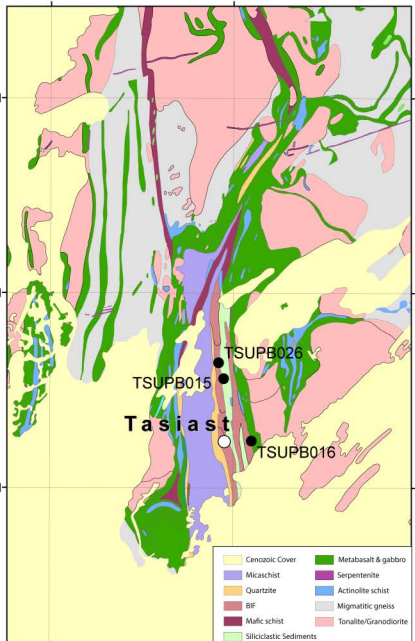
15°45'W
15°30'W
21°0'N
20°45'N
20°30'N
TSUPB026
TSUPB015
Tasiast
TSUPB016
Cenozoic Cover
Micaschist
Quartzite
BIF
Mafic schist
Siliciclastic Sediments
Metabasalt & gabbro
Serpentenite
Actinolite schist
Migmatitic gneiss
Tonalite/Granodiorite
0 2.5 5 10 15 20
Kilometers

a

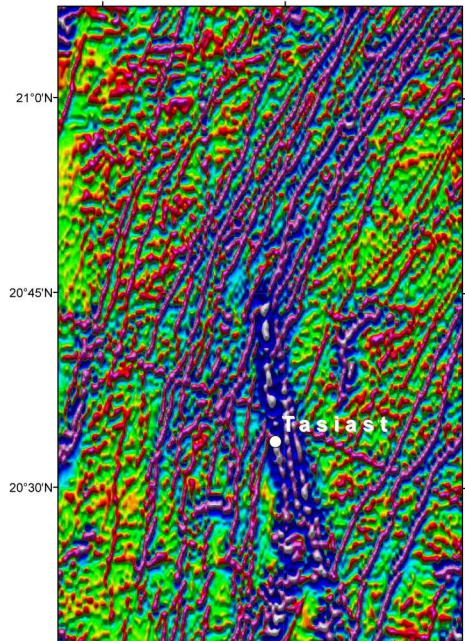
15°45'W
15°30'W
21°0'N
20°45'N
20°30'N
Tasiast
0 2.5 5 10 15 20
Kilometers

b

Figure 2

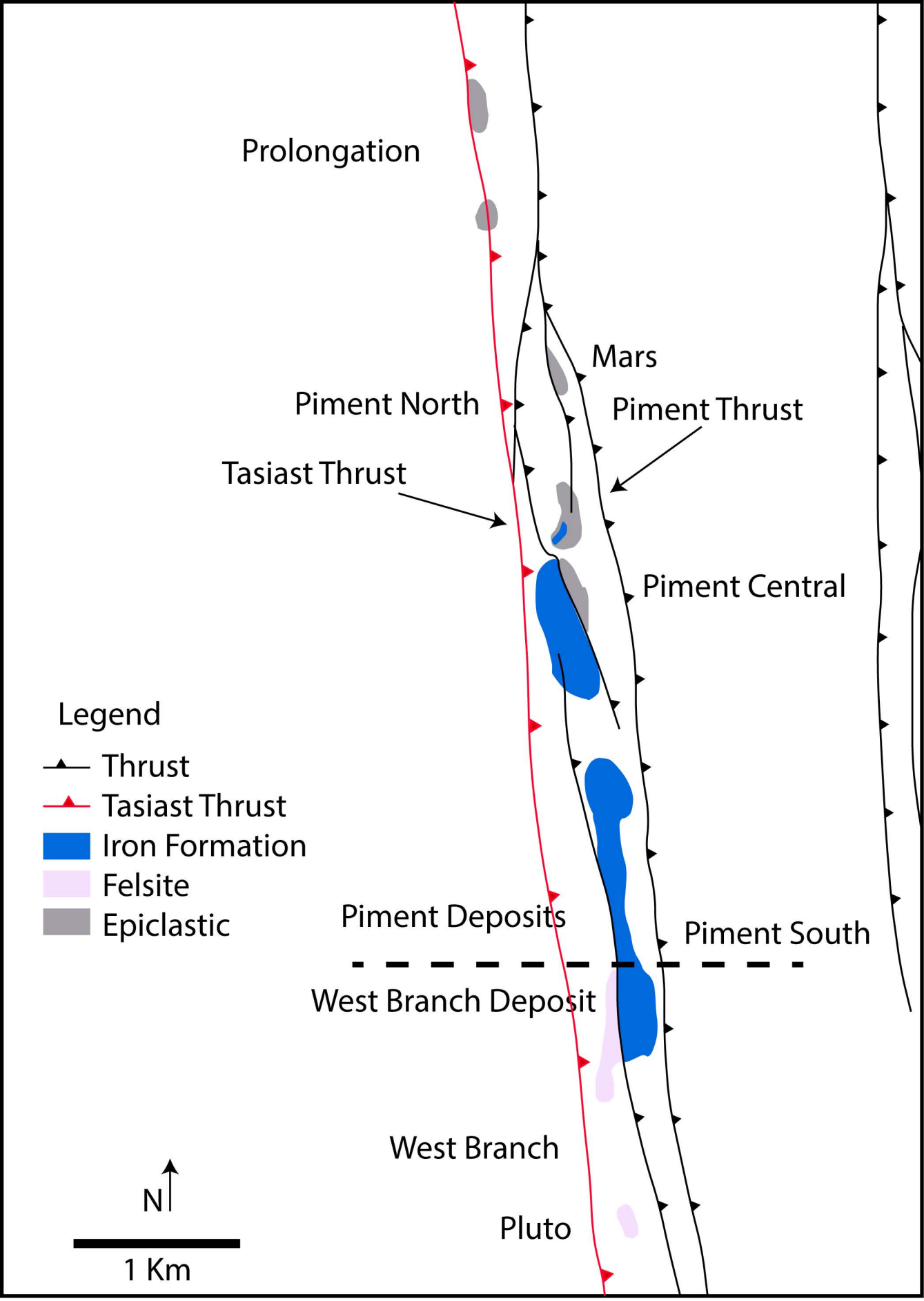
Prolongation
Mars
Piment North
Piment Thrust
Tasiast Thrust
Piment Central
Legend
Thrust
Tasiast Thrust
Iron Formation
Felsite
Epiclastic
Piment Deposits
Piment South
West Branch Deposit
West Branch
Pluto
N
1 Km

Figure 3

Figure 4

a

b

c

Figure 5

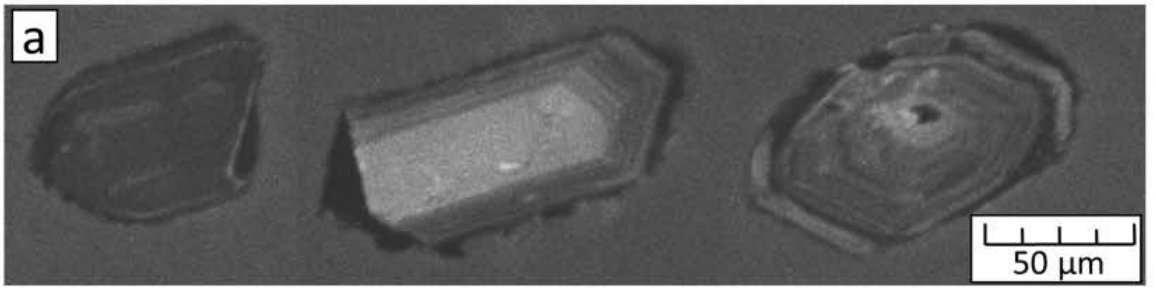

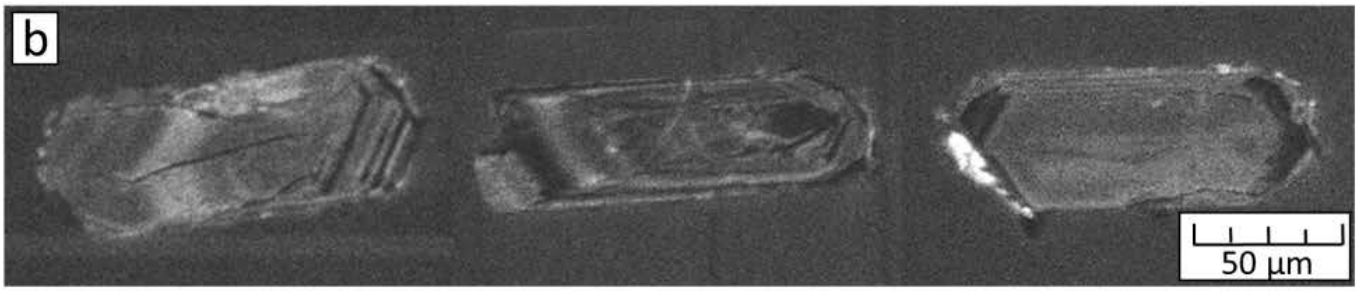

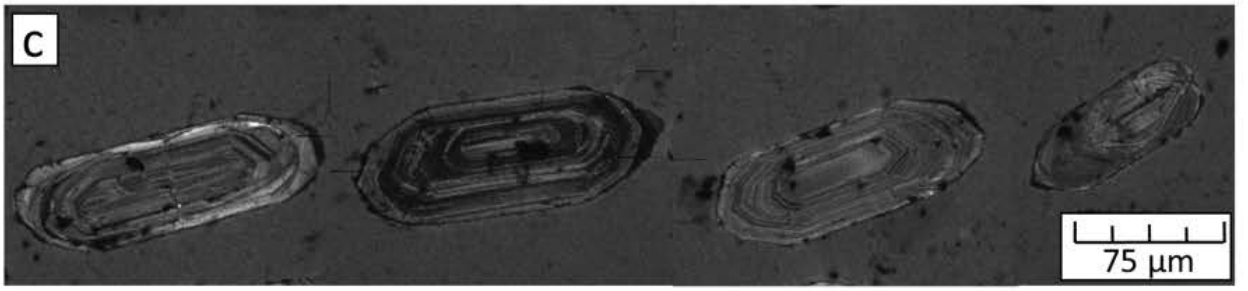

Figure 6

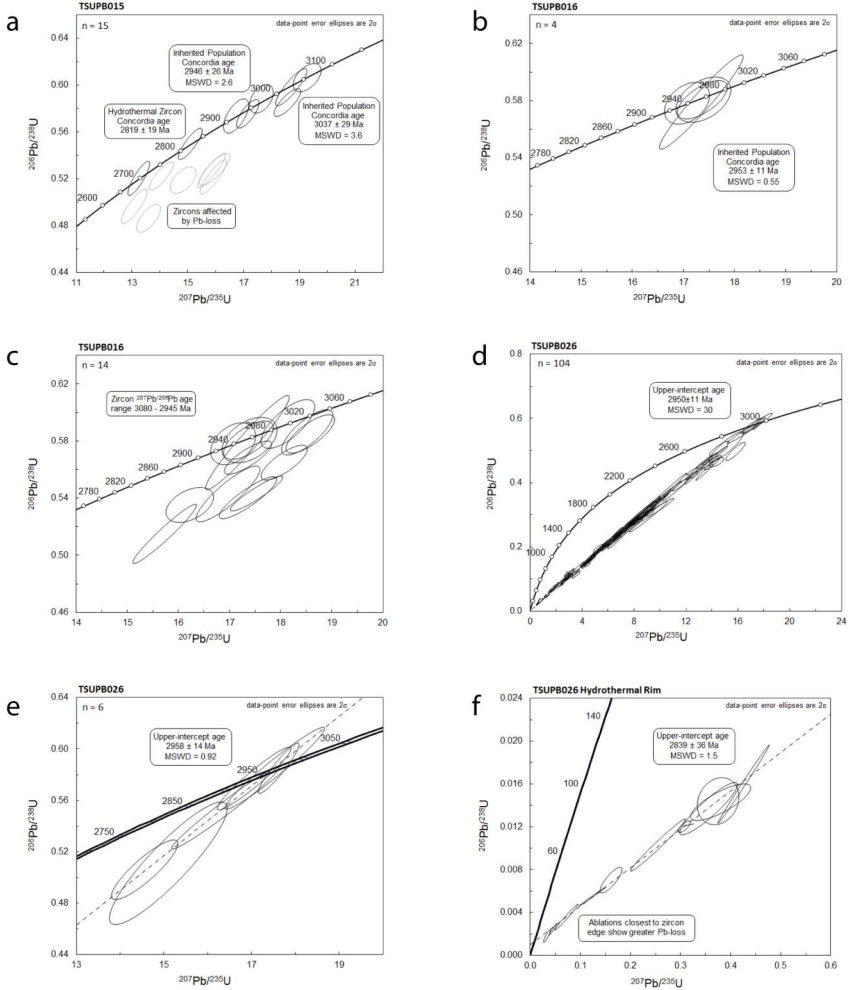
a
TSUPB015
n = 15
data-point error ellipses are 2σ
Inherited Population
Concordia age
2946 ± 26 Ma
MSWD = 2.6
Hydrothermal Zircon
Concordia age
2819 ± 19 Ma
Inherited Population
Concordia age
3037 ± 29 Ma
MSWD = 3.6
Zircons affected
by Pb-loss
b
TSUPB016
n = 4
data-point error ellipses are 2σ
Inherited Population
Concordia age
2953 ± 11 Ma
MSWD = 0.55
c
TSUPB016
n = 14
data-point error ellipses are 2σ
Zircon 207Pb/206Pb age
range 3080 - 2945 Ma
d
TSUPB026
n = 104
data-point error ellipses are 2σ
Upper-intercept age
2950±11 Ma
MSWD = 30
e
TSUPB026
n = 6
data-point error ellipses are 2σ
Upper-intercept age
2958 ± 14 Ma
MSWD = 0.92
f
TSUPB026 Hydrothermal Rim
data-point error ellipses are 2σ
Upper-intercept age
2839 ± 36 Ma
MSWD = 1.5
Ablations closest to zircon
edge show greater Pb-loss
206Pb/238U
207Pb/235U

Figure 7

Supplementary Material Table 1

	Concentration (ppm)	Ratios								Age (Ma)						
Sample	U	Th/U	$^{207}Pb/^{235}U$	Err 2SE abs	$^{206}Pb/^{238}U$	Err 2SE abs	Rho	$^{207}Pb/^{206}Pb$	Err 2SE abs	$^{207}Pb/^{235}U$	Err 2SE abs	$^{206}Pb/^{238}U$	Err 2SE abs	$^{207}Pb/^{206}Pb$	Err 2SE abs	% Discordant
TSUPB015_1	634	0.97	9.100	0.320	0.3699	0.0110	0.92	0.1710	0.0100	2346.0	33.0	2028.0	53.0	2568.0	10.0	18.1
TSUPB015_2	191	0.73	13.240	0.320	0.5203	0.0120	0.86	0.1747	0.0100	2696.0	23.0	2699.0	50.0	2600.1	9.1	3.3
TSUPB015_3	357	0.89	9.080	0.290	0.3514	0.0096	0.88	0.1759	0.0100	2345.0	29.0	1941.0	46.0	2621.0	8.0	24.7
TSUPB015_4	444	0.68	14.050	0.360	0.5224	0.0099	0.84	0.1876	0.0110	2753.0	25.0	2709.0	42.0	2720.8	9.9	2.6
TSUPB015_5	369	0.49	13.080	0.380	0.4964	0.0120	0.85	0.1887	0.0110	2684.0	28.0	2597.0	52.0	2729.0	10.0	4.9
TSUPB015_6	354	1.09	15.090	0.350	0.5498	0.0110	0.85	0.1895	0.0100	2821.0	22.0	2824.0	46.0	2743.2	6.2	1.4
TSUPB015_7	679	0.49	12.180	0.330	0.4449	0.0110	0.87	0.1910	0.0100	2620.0	24.0	2372.0	48.0	2753.3	8.4	13.8
TSUPB015_8	585	0.65	13.590	0.350	0.4862	0.0098	0.68	0.1940	0.0110	2721.0	24.0	2554.0	42.0	2791.9	8.8	9.1
TSUPB015_9	162	2.67	3.255	0.360	0.1189	0.0095	0.62	0.2013	0.0140	1469.0	84.0	724.0	54.0	2825.0	23.0	66.9
TSUPB015_10	531	1.01	11.010	0.320	0.3940	0.0089	0.59	0.2012	0.0100	2524.0	27.0	2141.0	41.0	2837.2	6.0	23.0
TSUPB015_11	281	0.72	14.830	0.380	0.5188	0.0092	0.54	0.2066	0.0120	2804.0	24.0	2694.0	39.0	2869.0	19.0	6.3
TSUPB015_12	547	0.87	13.600	0.400	0.4724	0.0110	0.94	0.2060	0.0130	2720.0	28.0	2493.0	50.0	2878.0	12.0	12.8
TSUPB015_13	220	0.66	12.640	0.350	0.4424	0.0099	0.73	0.2074	0.0120	2652.0	26.0	2361.0	44.0	2885.0	11.0	16.5
TSUPB015_14	182	0.48	12.680	0.540	0.4330	0.0140	0.87	0.2066	0.0120	2652.0	39.0	2317.0	65.0	2889.0	30.0	20.3
TSUPB015_15	384	0.99	17.150	0.330	0.5755	0.0100	0.76	0.2105	0.0130	2943.1	18.0	2930.0	43.0	2908.2	9.2	2.1
TSUPB015_16	661	0.80	12.920	0.510	0.4310	0.0140	0.95	0.2116	0.0110	2675.0	35.0	2308.0	62.0	2916.0	18.0	21.3
TSUPB015_17	417	0.55	16.730	0.370	0.5737	0.0120	0.62	0.2118	0.0130	2920.0	22.0	2923.0	48.0	2920.0	17.0	2.3
TSUPB015_18	736	0.90	13.830	0.350	0.4739	0.0110	0.87	0.2121	0.0110	2737.0	25.0	2500.0	49.0	2920.0	12.0	13.5
TSUPB015_19	659	1.04	12.220	0.420	0.4230	0.0140	0.95	0.2118	0.0120	2618.0	33.0	2272.0	64.0	2923.9	7.0	20.4
TSUPB015_20	484	1.10	11.470	0.340	0.3663	0.0120	0.74	0.2148	0.0110	2561.0	28.0	2011.0	56.0	2938.0	23.0	34.2
TSUPB015_21	301	0.57	17.640	0.350	0.5884	0.0100	0.44	0.2150	0.0130	2970.2	19.0	2983.0	41.0	2941.0	11.0	1.9
TSUPB015_22	662	0.99	15.850	0.410	0.5271	0.0120	0.90	0.2160	0.0130	2867.0	25.0	2729.0	50.0	2947.4	7.9	7.5
TSUPB015_23	492	0.99	11.670	0.300	0.3881	0.0110	0.68	0.2159	0.0110	2578.5	24.0	2113.0	50.0	2948.3	9.4	28.5
TSUPB015_24	815	1.06	10.990	0.720	0.3590	0.0150	0.94	0.2194	0.0130	2525.0	61.0	1977.0	71.0	2968.0	31.0	35.2
TSUPB015_25	546	0.39	15.920	0.390	0.5216	0.0120	0.88	0.2206	0.0120	2872.0	24.0	2706.0	51.0	2980.9	8.1	9.6
TSUPB015_26	822	0.53	13.050	0.550	0.4400	0.0200	0.97	0.2207	0.0120	2681.0	40.0	2349.0	88.0	2992.0	18.0	19.6
TSUPB015_27	497	0.81	15.960	0.450	0.5279	0.0110	0.81	0.2217	0.0130	2873.0	26.0	2732.0	47.0	2994.0	16.0	8.4
TSUPB015_28	326	0.62	18.710	0.460	0.5983	0.0130	0.88	0.2289	0.0140	3026.0	24.0	3022.0	51.0	3047.4	8.5	3.7
TSUPB015_29	405	0.56	18.570	0.390	0.5852	0.0097	0.80	0.2310	0.0130	3019.5	20.0	2970.0	39.0	3059.1	8.3	2.9
TSUPB015_30	357	0.58	19.280	0.410	0.6065	0.0099	0.51	0.2311	0.0140	3057.3	20.0	3056.0	40.0	3060.2	5.3	1.6
TSUPB015_31	358	0.53	14.250	0.410	0.4458	0.0098	0.59	0.2310	0.0140	2767.0	27.0	2376.0	44.0	3061.0	12.0	22.9
TSUPB015_32	776	1.32	11.400	0.500	0.3591	0.0120	0.92	0.2321	0.0120	2551.0	39.0	1977.0	56.0	3066.0	16.0	36.0
TSUPB015_33	360	1.17	17.340	0.410	0.5365	0.0098	0.64	0.2331	0.0140	2953.5	23.0	2768.0	41.0	3072.2	6.8	10.3
TSUPB015_34	533	0.46	16.640	0.580	0.5110	0.0140	0.93	0.2354	0.0140	2913.0	33.0	2661.0	62.0	3090.0	39.0	13.8
TSUPB015_35	577	0.78	17.400	0.430	0.5377	0.0110	0.73	0.2374	0.0140	2956.0	24.0	2774.0	48.0	3101.0	15.0	10.1
TSUPB015_36	294	0.96	16.160	0.470	0.4954	0.0110	0.92	0.2395	0.0140	2885.0	28.0	2594.0	46.0	3114.0	15.0	16.7
TSUPB015_37	1890	0.85	6.380	0.420	0.1926	0.0110	0.87	0.2416	0.0140	2024.0	56.0	1135.0	57.0	3136.0	27.0	69.9
TSUPB015_38	729	0.39	14.590	0.450	0.4354	0.0110	0.80	0.2475	0.0140	2788.0	29.0	2330.0	51.0	3164.0	13.0	28.1

TSUPB015_39	817	0.44	13.470	0.560	0.3890	0.0140	0.90	0.2555	0.0140	2710.0	39.0	2125.0	61.0	3222.0	17.0	37.7
TSUPB015_40	2374	1.61	12.240	0.580	0.3530	0.0140	0.99	0.2571	0.0120	2622.0	44.0	1948.0	69.0	3227.0	46.0	42.3
TSUPB015_41	1378	1.02	10.910	0.390	0.3164	0.0120	0.87	0.2585	0.0120	2514.0	34.0	1771.0	59.0	3238.0	15.0	50.2
TSUPB015_42	313	0.91	11.420	0.480	0.3188	0.0110	0.94	0.2595	0.0130	2562.0	40.0	1788.0	53.0	3247.0	10.0	52.8
TSUPB015_43	910	1.12	13.000	0.510	0.3498	0.0120	0.97	0.2663	0.0140	2678.0	38.0	1933.0	59.0	3279.0	17.0	49.3
TSUPB016_1	801	0.29	5.110	0.590	0.1680	0.0150	1.00	0.2097	0.0130	1833.0	96.0	997.0	83.0	2904.0	30.0	65.7
TSUPB016_2	3800	0.09	1.720	0.360	0.0557	0.0089	0.93	0.2140	0.0150	1006.0	140.0	349.0	54.0	2925.0	50.0	77.3
TSUPB016_3	366	0.27	15.240	0.410	0.4993	0.0110	0.86	0.2122	0.0130	2830.0	25.0	2611.0	48.0	2928.0	10.0	11.9
TSUPB016_4	1443	0.15	9.120	0.430	0.3054	0.0130	0.98	0.2138	0.0130	2346.0	43.0	1716.0	64.0	2934.0	6.1	42.2
TSUPB016_5	207	0.47	17.370	0.400	0.5806	0.0110	0.65	0.2160	0.0130	2955.0	22.0	2951.0	46.0	2942.5	6.1	2.0
TSUPB016_6	325	0.32	15.240	0.420	0.4999	0.0130	0.73	0.2163	0.0140	2830.0	26.0	2613.0	55.0	2949.0	6.0	12.8
TSUPB016_7	375	0.34	15.730	0.510	0.5150	0.0170	0.96	0.2167	0.0130	2859.0	31.0	2676.0	72.0	2955.2	4.4	9.6
TSUPB016_8	272	0.46	17.360	0.380	0.5684	0.0095	0.82	0.2166	0.0130	2954.6	21.0	2901.0	39.0	2958.8	6.7	2.8
TSUPB016_9	458	0.29	17.350	0.670	0.5790	0.0270	0.96	0.2191	0.0130	2952.0	38.0	2940.0	110.0	2973.0	10.0	6.5
TSUPB016_10	168	0.45	17.390	0.440	0.5807	0.0130	0.43	0.2193	0.0130	2956.0	24.0	2951.0	53.0	2977.0	17.0	3.2
TSUPB016_11	208	0.19	12.680	0.380	0.4168	0.0097	0.70	0.2191	0.0140	2656.0	28.0	2246.0	44.0	2980.0	13.0	24.6
TSUPB016_12	295	0.36	10.380	0.540	0.3320	0.0140	0.86	0.2211	0.0130	2462.0	48.0	1847.0	66.0	2981.0	14.0	38.3
TSUPB016_13	384	0.46	13.700	0.410	0.4616	0.0100	0.69	0.2194	0.0130	2729.0	28.0	2446.0	45.0	2982.0	12.0	15.8
TSUPB016_14	521	0.50	11.020	0.470	0.3584	0.0120	0.91	0.2203	0.0130	2529.0	41.0	1973.0	58.0	2982.0	20.0	35.2
TSUPB016_15	359	0.33	17.070	0.360	0.5781	0.0120	0.37	0.2228	0.0130	2938.8	20.0	2941.0	47.0	2999.0	9.5	1.8
TSUPB016_16	178	0.28	18.580	0.390	0.5850	0.0110	0.76	0.2224	0.0130	3020.0	20.0	2969.0	44.0	3001.6	8.6	2.5
TSUPB016_17	218	0.30	18.520	0.410	0.5862	0.0130	0.77	0.2230	0.0140	3019.0	21.0	2973.0	53.0	3005.0	14.0	4.0
TSUPB016_18	277	0.34	18.140	0.430	0.5920	0.0140	0.71	0.2247	0.0140	2997.0	23.0	2996.0	59.0	3020.0	14.0	3.2
TSUPB016_19	161	0.25	18.070	0.370	0.5649	0.0100	0.78	0.2268	0.0140	2993.0	20.0	2886.0	42.0	3024.6	6.9	6.1
TSUPB016_20	404	0.33	16.220	0.380	0.5353	0.0100	0.44	0.2266	0.0130	2892.0	25.0	2764.0	42.0	3030.5	9.4	7.0
TSUPB016_21	457	0.35	14.770	0.520	0.4740	0.0150	0.91	0.2294	0.0130	2804.0	32.0	2498.0	66.0	3045.6	7.3	17.3
TSUPB016_22	320	0.49	16.210	0.400	0.4943	0.0110	0.70	0.2295	0.0130	2889.0	24.0	2589.0	46.0	3050.2	7.8	17.0
TSUPB016_23	432	0.25	16.020	0.390	0.5183	0.0130	0.88	0.2297	0.0130	2878.0	23.0	2691.0	54.0	3055.0	15.0	10.9
TSUPB016_24	512	0.43	12.160	0.400	0.3823	0.0100	0.93	0.2311	0.0140	2615.0	31.0	2087.0	47.0	3055.0	17.0	33.2
TSUPB016_25	136	0.17	17.360	0.460	0.5403	0.0120	0.88	0.2301	0.0140	2954.0	25.0	2784.0	48.0	3057.5	6.8	9.3
TSUPB016_26	1370	0.34	4.698	0.350	0.1447	0.0096	0.80	0.2314	0.0140	1766.0	61.0	871.0	54.0	3059.0	28.0	74.4
TSUPB016_27	533	0.68	17.530	0.420	0.5433	0.0100	0.93	0.2317	0.0130	2963.0	23.0	2797.0	42.0	3061.6	5.9	9.3
TSUPB016_28	89	0.21	14.840	0.380	0.4792	0.0097	0.27	0.2317	0.0140	2805.0	24.0	2524.0	42.0	3065.0	13.0	16.1
TSUPB016_29	1307	0.09	5.280	0.640	0.1500	0.0140	0.85	0.2340	0.0160	1835.0	110.0	899.0	78.0	3067.0	65.0	77.0
TSUPB016_30	366	0.31	16.970	0.510	0.5430	0.0160	0.88	0.2355	0.0140	2932.0	29.0	2797.0	67.0	3083.0	20.0	8.0
TSUPB016_31	951	0.25	4.433	0.340	0.1358	0.0088	0.37	0.2341	0.0140	1718.4	63.0	821.0	50.0	3083.0	21.0	77.8
TSUPB016_32	474	0.11	3.960	0.350	0.1205	0.0091	0.97	0.2337	0.0140	1623.0	72.0	733.0	52.0	3083.0	13.0	79.8
TSUPB016_33	166	0.13	15.950	0.380	0.5017	0.0096	0.60	0.2361	0.0140	2873.0	23.0	2621.0	41.0	3092.7	8.6	14.1
TSUPB016_34	385	0.49	15.010	0.370	0.4450	0.0096	0.69	0.2359	0.0130	2816.0	24.0	2373.0	43.0	3093.0	12.0	26.8
TSUPB016_35	952	0.31	8.840	0.390	0.2673	0.0110	0.95	0.2386	0.0140	2319.0	41.0	1526.0	58.0	3094.0	24.0	56.9

TSUPB016_36	234	0.20	14.960	0.410	0.4707	0.0110	0.88	0.2394	0.0140	2813.0	26.0	2487.0	50.0	3115.0	11.0	18.8
TSUPB016_37	243	0.24	12.510	0.390	0.3761	0.0110	0.90	0.2424	0.0140	2647.0	32.0	2057.0	50.0	3136.0	11.0	37.6
TSUPB016_38	311	0.33	19.480	0.440	0.5651	0.0110	0.65	0.2439	0.0130	3065.0	22.0	2887.0	45.0	3146.0	16.0	10.9
TSUPB016_39	952	0.36	6.498	0.340	0.1896	0.0089	0.87	0.2450	0.0130	2045.0	47.0	1119.0	48.0	3151.7	6.8	73.0
TSUPB016_40	791	0.40	13.520	0.440	0.4070	0.0160	0.97	0.2451	0.0130	2716.0	31.0	2200.0	74.0	3156.0	12.0	31.9
TSUPB016_41	618	0.44	11.070	0.390	0.3208	0.0089	0.63	0.2459	0.0140	2529.0	33.0	1794.0	44.0	3158.0	15.0	50.0
TSUPB016_42	636	0.34	13.330	0.490	0.4080	0.0140	0.72	0.2462	0.0150	2703.0	35.0	2204.0	66.0	3162.0	36.0	29.7
TSUPB016_43	538	0.20	8.650	0.550	0.2407	0.0093	0.57	0.2530	0.0170	2296.0	58.0	1390.0	48.0	3194.0	64.0	67.4
TSUPB016_44	220	0.12	14.100	0.440	0.3930	0.0150	0.89	0.2563	0.0140	2756.0	30.0	2138.0	70.0	3218.0	25.0	40.2
TSUPB016_45	619	0.72	13.770	0.520	0.3699	0.0110	0.70	0.2611	0.0140	2733.0	35.0	2029.0	53.0	3264.0	22.0	45.8
TSUPB016_46	282	0.18	19.360	0.420	0.5340	0.0150	0.29	0.2668	0.0150	3060.0	21.0	2755.0	65.0	3287.0	38.0	15.7
TSUPB016_47	1137	0.58	8.340	0.370	0.2249	0.0090	0.85	0.2706	0.0130	2267.0	40.0	1310.0	50.0	3307.0	16.0	73.6
TSUPB016_48	813	0.26	12.230	0.460	0.3123	0.0120	0.97	0.2842	0.0140	2619.0	37.0	1751.0	60.0	3380.0	15.0	61.1
TSUPB026_1	2950	1.17	0.720	0.091	0.0355	0.0041	0.95	0.1461	0.0025	548.0	55.0	225.0	26.0	2301.0	29.0	90.3
TSUPB026_2	4000	0.50	0.608	0.076	0.0260	0.0029	0.93	0.1702	0.0055	478.0	48.0	165.0	18.0	2556.0	55.0	93.6
TSUPB026_3	1400	1.50	1.200	0.056	0.0491	0.0031	0.92	0.1724	0.0041	799.0	25.0	309.0	19.0	2578.0	39.0	88.1
TSUPB026_4	1100	0.12	2.790	0.120	0.1163	0.0066	0.94	0.1720	0.0037	1360.0	36.0	709.0	38.0	2582.0	34.0	72.1
TSUPB026_5	5200	0.62	0.580	0.100	0.0229	0.0034	0.99	0.1735	0.0041	453.0	67.0	146.0	21.0	2590.0	39.0	94.4
TSUPB026_6	1120	0.28	2.020	0.140	0.0817	0.0065	0.94	0.1771	0.0035	1116.0	48.0	506.0	39.0	2625.0	33.0	81.2
TSUPB026_7	1020	0.21	1.720	0.240	0.0712	0.0093	0.97	0.1773	0.0050	999.0	94.0	442.0	56.0	2625.0	48.0	83.2
TSUPB026_8	1020	0.23	1.134	0.045	0.0464	0.0020	0.83	0.1773	0.0036	769.0	21.0	292.0	12.0	2626.0	33.0	88.8
TSUPB026_9	1110	0.14	0.962	0.028	0.0389	0.0010	0.50	0.1790	0.0045	684.0	15.0	246.2	5.9	2642.0	42.0	90.7
TSUPB026_10	420	0.22	1.530	0.130	0.0615	0.0055	0.89	0.1823	0.0070	935.0	52.0	384.0	33.0	2668.0	64.0	85.5
TSUPB026_11	1180	0.41	1.757	0.056	0.0699	0.0017	0.89	0.1829	0.0033	1029.0	20.0	436.0	10.0	2679.0	30.0	83.6
TSUPB026_12	3480	0.47	0.211	0.028	0.0083	0.0011	0.97	0.1836	0.0065	194.0	23.0	53.3	7.2	2682.0	57.0	98.0
TSUPB026_13	2120	0.47	3.040	0.310	0.1200	0.0110	0.98	0.1836	0.0034	1402.0	91.0	731.0	64.0	2685.0	30.0	73.0
TSUPB026_14	3280	0.41	0.607	0.036	0.0245	0.0014	0.97	0.1847	0.0036	481.0	23.0	155.8	8.6	2695.0	33.0	94.2
TSUPB026_15	1230	0.30	2.450	0.200	0.0946	0.0066	0.98	0.1850	0.0033	1251.0	60.0	582.0	39.0	2697.0	29.0	78.5
TSUPB026_16	668	0.33	3.150	0.160	0.1221	0.0062	0.85	0.1853	0.0035	1452.0	36.0	742.0	36.0	2700.0	32.0	72.6
TSUPB026_17	2700	0.69	0.322	0.017	0.0126	0.0006	0.95	0.1873	0.0044	283.0	13.0	80.5	3.8	2717.0	39.0	97.0
TSUPB026_18	1098	0.13	2.954	0.098	0.1145	0.0031	0.94	0.1871	0.0018	1393.0	25.0	699.0	18.0	2719.0	16.0	74.3
TSUPB026_19	2040	0.55	0.311	0.023	0.0123	0.0007	0.78	0.1883	0.0049	274.0	18.0	78.7	4.3	2721.0	43.0	97.2
TSUPB026_20	1220	0.34	2.170	0.084	0.0838	0.0039	0.90	0.1885	0.0030	1171.0	26.0	519.0	23.0	2729.0	27.0	81.0
TSUPB026_21	1440	0.49	2.010	0.140	0.0780	0.0050	0.95	0.1899	0.0047	1114.0	51.0	484.0	30.0	2739.0	41.0	82.2
TSUPB026_22	810	0.28	2.580	0.170	0.0965	0.0079	0.85	0.1876	0.0063	1289.0	50.0	593.0	46.0	2750.0	58.0	78.3
TSUPB026_23	1520	0.38	1.120	0.230	0.0408	0.0078	0.99	0.1954	0.0045	730.0	120.0	257.0	49.0	2786.0	38.0	90.9
TSUPB026_24	760	0.29	3.080	0.610	0.1070	0.0190	0.99	0.1956	0.0050	1400.0	140.0	690.0	130.0	2788.0	41.0	76.6
TSUPB026_25	1340	0.62	0.563	0.053	0.0206	0.0019	0.95	0.1978	0.0082	451.0	35.0	131.0	12.0	2801.0	68.0	95.3
TSUPB026_26	790	0.47	2.870	0.290	0.1060	0.0100	0.99	0.1972	0.0034	1380.0	87.0	648.0	61.0	2802.0	28.0	77.0
TSUPB026_27	402	0.47	6.730	0.320	0.2430	0.0140	0.93	0.1982	0.0032	2075.0	43.0	1403.0	72.0	2811.0	26.0	49.2

TSUPB026_28	627	0.39	3.780	0.340	0.1380	0.0130	0.95	0.1986	0.0047	1582.0	70.0	833.0	75.0	2813.0	39.0	71.3
TSUPB026_29	606	0.29	5.300	0.330	0.1950	0.0110	0.75	0.1986	0.0031	1863.0	56.0	1145.0	61.0	2814.0	25.0	59.5
TSUPB026_30	2110	0.26	1.670	0.160	0.0632	0.0059	0.97	0.1981	0.0050	1012.0	55.0	395.0	36.0	2818.0	36.0	85.9
TSUPB026_31	510	0.32	1.800	0.230	0.0659	0.0071	0.97	0.1988	0.0078	1045.0	75.0	411.0	43.0	2822.0	60.0	85.8
TSUPB026_32	510	0.37	2.890	0.200	0.1059	0.0068	0.94	0.1993	0.0057	1374.0	52.0	648.0	39.0	2827.0	49.0	77.6
TSUPB026_33	260	0.41	5.340	0.450	0.1940	0.0160	0.98	0.2009	0.0028	1844.0	76.0	1136.0	85.0	2831.0	23.0	60.0
TSUPB026_34	620	0.34	5.270	0.800	0.1890	0.0280	1.00	0.2008	0.0028	1830.0	140.0	1110.0	150.0	2832.0	23.0	60.9
TSUPB026_35	910	0.33	2.840	0.140	0.1023	0.0056	0.92	0.2010	0.0044	1363.0	39.0	628.0	33.0	2833.0	36.0	77.8
TSUPB026_36	570	0.15	5.900	0.260	0.2121	0.0091	0.81	0.2018	0.0031	1958.0	39.0	1239.0	48.0	2840.0	25.0	56.3
TSUPB026_37	1060	0.36	1.360	0.110	0.0481	0.0044	0.93	0.2016	0.0065	866.0	48.0	303.0	27.0	2848.0	56.0	89.3
TSUPB026_38	562	0.84	2.720	0.200	0.0981	0.0078	0.83	0.2037	0.0077	1340.0	59.0	603.0	46.0	2850.0	59.0	78.7
TSUPB026_39	580	1.02	4.250	0.330	0.1500	0.0094	0.96	0.2031	0.0031	1694.0	71.0	900.0	53.0	2851.0	25.0	68.7
TSUPB026_40	350	0.36	8.700	1.100	0.3130	0.0370	1.00	0.2032	0.0017	2290.0	120.0	1780.0	170.0	2852.0	14.0	37.8
TSUPB026_41	217	0.30	7.360	0.720	0.2600	0.0250	0.98	0.2023	0.0034	2158.0	89.0	1480.0	130.0	2852.0	31.0	48.1
TSUPB026_42	550	0.22	4.780	0.730	0.1720	0.0260	0.99	0.2038	0.0044	1750.0	150.0	1010.0	150.0	2862.0	33.0	64.4
TSUPB026_43	650	0.22	3.330	0.240	0.1162	0.0074	0.89	0.2052	0.0067	1481.0	55.0	708.0	43.0	2864.0	53.0	75.3
TSUPB026_44	4600	0.74	0.670	0.160	0.0239	0.0055	1.00	0.2050	0.0030	507.0	98.0	152.0	35.0	2866.0	24.0	94.7
TSUPB026_45	670	0.31	7.530	0.690	0.2690	0.0240	1.00	0.2057	0.0015	2166.0	90.0	1530.0	120.0	2872.0	12.0	46.6
TSUPB026_46	431	0.24	6.260	0.380	0.2220	0.0160	0.97	0.2060	0.0039	2007.0	55.0	1292.0	83.0	2873.0	32.0	55.6
TSUPB026_47	690	0.53	3.020	0.230	0.1073	0.0075	0.95	0.2048	0.0057	1404.0	64.0	656.0	44.0	2873.0	49.0	77.6
TSUPB026_48	500	0.45	7.250	0.580	0.2540	0.0200	0.99	0.2064	0.0033	2127.0	79.0	1450.0	110.0	2876.0	26.0	49.4
TSUPB026_49	440	0.29	7.100	1.300	0.2440	0.0370	0.98	0.2066	0.0047	2090.0	160.0	1400.0	190.0	2878.0	37.0	51.9
TSUPB026_50	570	0.33	6.600	1.200	0.2320	0.0390	1.00	0.2079	0.0024	2050.0	160.0	1330.0	210.0	2889.0	19.0	54.1
TSUPB026_51	690	0.29	4.260	0.270	0.1468	0.0091	0.97	0.2082	0.0044	1679.0	56.0	882.0	51.0	2889.0	34.0	69.6
TSUPB026_52	309	0.22	7.480	0.740	0.2580	0.0280	0.99	0.2074	0.0032	2148.0	96.0	1470.0	150.0	2890.0	26.0	49.0
TSUPB026_53	860	0.30	5.200	0.680	0.1820	0.0230	0.99	0.2084	0.0040	1800.0	150.0	1070.0	130.0	2891.0	31.0	62.9
TSUPB026_54	420	0.54	9.160	0.790	0.3200	0.0280	0.98	0.2087	0.0047	2344.0	84.0	1790.0	140.0	2894.0	37.0	39.8
TSUPB026_55	263	0.64	8.610	0.370	0.2990	0.0100	0.94	0.2089	0.0034	2294.0	40.0	1688.0	50.0	2896.0	26.0	41.8
TSUPB026_56	401	0.45	7.430	0.910	0.2560	0.0320	0.99	0.2091	0.0031	2150.0	120.0	1460.0	160.0	2898.0	24.0	49.4
TSUPB026_57	410	0.60	6.500	1.500	0.2310	0.0500	1.00	0.2093	0.0057	2010.0	210.0	1330.0	260.0	2899.0	45.0	54.1
TSUPB026_58	413	0.36	10.560	0.260	0.3695	0.0089	0.96	0.2097	0.0028	2492.0	28.0	2041.0	50.0	2902.0	22.0	29.5
TSUPB026_59	989	0.42	2.485	0.082	0.0850	0.0032	0.57	0.2098	0.0049	1267.0	24.0	526.0	19.0	2902.0	37.0	81.9
TSUPB026_60	533	0.16	9.340	0.310	0.3250	0.0120	0.96	0.2098	0.0017	2371.0	31.0	1813.0	58.0	2904.0	13.0	38.1
TSUPB026_61	290	0.42	9.000	0.530	0.3110	0.0170	0.97	0.2103	0.0037	2330.0	59.0	1741.0	84.0	2906.0	29.0	40.2
TSUPB026_62	220	0.41	4.560	0.390	0.1590	0.0140	0.95	0.2103	0.0043	1730.0	73.0	951.0	77.0	2906.0	33.0	67.7
TSUPB026_63	261	0.31	13.040	0.840	0.4460	0.0300	0.98	0.2104	0.0040	2672.0	67.0	2370.0	140.0	2907.0	31.0	18.5
TSUPB026_64	419	0.25	6.570	0.440	0.2290	0.0150	0.98	0.2103	0.0036	2048.0	60.0	1329.0	81.0	2907.0	28.0	55.1
TSUPB026_65	380	0.44	6.000	0.760	0.2080	0.0240	0.99	0.2108	0.0049	1970.0	120.0	1210.0	130.0	2909.0	37.0	58.5
TSUPB026_66	325	0.42	8.500	1.800	0.2980	0.0560	1.00	0.2107	0.0062	2260.0	200.0	1670.0	280.0	2910.0	47.0	42.7
TSUPB026_67	112	0.51	9.170	0.280	0.3049	0.0078	0.74	0.2110	0.0038	2354.0	28.0	1715.0	39.0	2913.0	29.0	41.4
TSUPB026_68	700	0.37	2.340	0.160	0.0802	0.0044	0.94	0.2108	0.0040	1232.0	50.0	497.0	26.0	2918.0	27.0	83.0
TSUPB026_69	301	0.31	8.510	0.420	0.2950	0.0120	0.87	0.2120	0.0048	2282.0	46.0	1666.0	58.0	2919.0	37.0	42.6

TSUPB026_70	389	0.32	9.820	0.470	0.3420	0.0130	0.98	0.2121	0.0028	2414.0	46.0	1897.0	65.0	2921.0	21.0	34.6
TSUPB026_71	458	0.64	6.670	0.570	0.2210	0.0220	0.97	0.2125	0.0064	2055.0	79.0	1310.0	110.0	2921.0	49.0	58.2
TSUPB026_72	362	1.08	4.560	0.470	0.1580	0.0150	0.99	0.2125	0.0029	1713.0	87.0	938.0	84.0	2923.0	22.0	68.0
TSUPB026_73	204	0.44	15.100	1.100	0.5110	0.0390	0.90	0.2135	0.0080	2808.0	73.0	2650.0	170.0	2925.0	63.0	9.3
TSUPB026_74	537	0.40	5.800	0.250	0.1980	0.0085	0.94	0.2130	0.0035	1944.0	37.0	1164.0	46.0	2927.0	26.0	60.4
TSUPB026_75	509	0.50	4.820	0.170	0.1641	0.0066	0.88	0.2130	0.0045	1787.0	31.0	979.0	37.0	2927.0	34.0	66.6
TSUPB026_76	299	0.33	12.820	0.410	0.4310	0.0140	0.92	0.2133	0.0037	2665.0	31.0	2311.0	66.0	2930.0	28.0	22.0
TSUPB026_77	480	0.51	9.700	1.600	0.3390	0.0540	1.00	0.2138	0.0025	2420.0	150.0	1860.0	270.0	2934.0	19.0	36.3
TSUPB026_78	319	0.37	8.720	0.890	0.3060	0.0320	0.96	0.2140	0.0046	2360.0	68.0	1710.0	160.0	2934.0	34.0	41.1
TSUPB026_79	70	0.47	14.560	0.620	0.5060	0.0190	0.88	0.2140	0.0039	2785.0	40.0	2640.0	82.0	2935.0	30.0	8.5
TSUPB026_80	338	0.44	8.900	0.980	0.3080	0.0350	0.97	0.2144	0.0064	2300.0	120.0	1720.0	180.0	2935.0	48.0	40.8
TSUPB026_81	420	0.50	9.010	0.510	0.3030	0.0150	0.98	0.2144	0.0036	2332.0	56.0	1703.0	77.0	2937.0	27.0	43.2
TSUPB026_82	266	0.70	14.250	0.800	0.4840	0.0240	0.99	0.2144	0.0026	2758.0	57.0	2540.0	110.0	2938.0	20.0	13.7
TSUPB026_83	248	0.25	8.520	0.720	0.2920	0.0230	0.97	0.2144	0.0043	2275.0	82.0	1640.0	120.0	2938.0	33.0	43.8
TSUPB026_84	172	0.32	13.620	0.670	0.4680	0.0200	0.96	0.2145	0.0022	2720.0	47.0	2471.0	86.0	2939.0	17.0	15.7
TSUPB026_85	175	0.43	11.630	0.530	0.3950	0.0170	0.96	0.2146	0.0033	2571.0	44.0	2142.0	78.0	2940.0	25.0	27.2
TSUPB026_86	189	0.87	7.720	0.270	0.2605	0.0099	0.97	0.2146	0.0022	2194.0	33.0	1490.0	51.0	2946.0	15.0	49.2
TSUPB026_87	463	0.45	9.500	1.300	0.3100	0.0340	0.98	0.2159	0.0018	2370.0	120.0	1830.0	240.0	2950.0	13.0	41.1
TSUPB026_88	500	0.31	9.500	2.100	0.3350	0.0780	1.00	0.2160	0.0064	2370.0	210.0	1850.0	380.0	2951.0	47.0	37.0
TSUPB026_89	183	0.35	17.060	0.690	0.5770	0.0200	0.95	0.2169	0.0036	2935.0	40.0	2932.0	84.0	2956.0	27.0	1.0
TSUPB026_90	500	0.29	6.450	0.440	0.2180	0.0140	0.96	0.2170	0.0051	2032.0	62.0	1271.0	75.0	2956.0	37.0	57.0
TSUPB026_91	354	0.18	11.290	0.900	0.3820	0.0320	0.98	0.2170	0.0035	2535.0	78.0	2080.0	150.0	2957.0	26.0	29.4
TSUPB026_92	189	0.40	13.400	1.100	0.4540	0.0250	0.97	0.2174	0.0045	2691.0	81.0	2410.0	110.0	2960.0	33.0	19.1
TSUPB026_93	352	0.34	12.420	0.430	0.4160	0.0170	0.95	0.2174	0.0028	2634.0	33.0	2240.0	79.0	2961.0	21.0	24.5
TSUPB026_94	576	0.44	4.370	0.310	0.1490	0.0130	0.95	0.2180	0.0092	1702.0	56.0	892.0	75.0	2961.0	67.0	69.7
TSUPB026_95	156	0.25	17.530	0.930	0.5850	0.0260	0.97	0.2179	0.0042	2958.0	54.0	2970.0	110.0	2964.0	31.0	-0.3
TSUPB026_96	168	0.25	16.400	1.000	0.5540	0.0260	0.98	0.2180	0.0029	2890.0	66.0	2840.0	110.0	2965.0	21.0	4.6
TSUPB026_97	583	0.30	4.420	0.180	0.1457	0.0058	0.80	0.2196	0.0063	1714.0	35.0	876.0	32.0	2976.0	46.0	70.1
TSUPB026_98	248	0.51	13.430	0.550	0.4330	0.0210	0.98	0.2205	0.0036	2707.0	40.0	2316.0	94.0	2983.0	26.0	22.8
TSUPB026_99	167	0.35	17.620	0.380	0.5850	0.0160	0.94	0.2211	0.0027	2969.0	21.0	2970.0	64.0	2988.0	20.0	0.1
TSUPB026_100	249	0.50	14.370	0.440	0.4640	0.0120	0.68	0.2229	0.0056	2773.0	29.0	2456.0	55.0	3012.0	36.0	18.4
TSUPB026_101	524	0.17	3.550	0.260	0.1133	0.0090	0.94	0.2248	0.0056	1534.0	58.0	692.0	52.0	3014.0	40.0	77.0
TSUPB026_102	840	0.59	9.100	1.200	0.2940	0.0390	0.98	0.2250	0.0044	2370.0	130.0	1640.0	200.0	3015.0	31.0	45.7
TSUPB026_103	221	0.41	13.990	0.470	0.4580	0.0150	0.92	0.2254	0.0034	2747.0	32.0	2430.0	68.0	3019.0	24.0	19.9
TSUPB026_104	287	0.51	15.820	0.610	0.4970	0.0230	0.89	0.2280	0.0051	2864.0	38.0	2622.0	91.0	3036.0	36.0	14.6
TSUPB026_Rim_1	22900	0.51	0.045	0.006	0.0024	0.0004	0.97	0.1434	0.0069	44.7	6.0	15.6	2.8	2268.0	83.0	99.3
TSUPB026_Rim_2	29000	0.46	0.033	0.006	0.0018	0.0005	0.90	0.1440	0.0150	33.1	5.4	11.5	3.0	2280.0	180.0	99.5
TSUPB026_Rim_3	16900	0.47	0.072	0.019	0.0036	0.0010	0.99	0.1541	0.0062	71.0	18.0	22.9	6.3	2392.0	68.0	99.0
TSUPB026_Rim_4	9600	0.46	0.124	0.022	0.0055	0.0007	1.00	0.1701	0.0069	119.0	20.0	35.3	4.7	2557.0	68.0	98.6
TSUPB026_Rim_5	6900	0.45	0.161	0.018	0.0070	0.0010	0.83	0.1720	0.0200	151.0	15.0	45.1	6.4	2570.0	200.0	98.2

TSUPB026_Rim_6	4060	0.47	0.255	0.045	0.0103	0.0020	0.99	0.1847	0.0088	230.0	37.0	66.0	12.0	2694.0	79.0	97.6
TSUPB026_Rim_7	1970	0.51	0.307	0.010	0.0120	0.0004	0.74	0.1870	0.0130	272.1	7.5	77.0	2.8	2710.0	110.0	97.2
TSUPB026_Rim_8	1850	0.52	0.356	0.047	0.0137	0.0020	0.91	0.1905	0.0076	309.0	35.0	88.0	13.0	2746.0	65.0	96.8
TSUPB026_Rim_9	2273	0.56	0.375	0.034	0.0144	0.0018	0.18	0.1950	0.0360	323.0	25.0	92.0	12.0	2760.0	320.0	96.6
TSUPB026_Rim_10	2970	0.52	0.317	0.008	0.0122	0.0001	1.00	0.1924	0.0033	279.3	6.2	78.1	0.5	2762.0	28.0	97.2
TSUPB026_Rim_11	2170	0.50	0.380	0.049	0.0143	0.0014	0.78	0.1952	0.0057	327.0	36.0	91.5	9.0	2786.0	48.0	96.7
TSUPB026_Rim_12	1750	0.61	0.426	0.042	0.0160	0.0030	1.00	0.1960	0.0170	360.0	30.0	102.0	19.0	2790.0	140.0	96.3